Length of the tightest trefoil knot

Justyna Baranska, Piotr Pieranski,* and Sylwester Przybyl
Laboratory of Computational and Semiconductor Physics, Poznan University of Technology, Nieszawska 5B/11, 60-965 Poznan, Poland

Eric J. Rawdon†
Department of Mathematics and Computer Science, Duquesne University, Pittsburgh, Pennsylvania 15282, USA
(Received 23 August 2004; published 29 November 2004)

The physical sense of tight knots provided by the SONO algorithm is discussed. A method allowing one to predict their length is presented. An upper bound for the minimum length of a smooth trefoil knot is determined.

DOI: 10.1103/PhysRevE.70.051810 PACS number(s): 36.20.−r, 46.70.−p, 87.19.−j

I. INTRODUCTION

The conformations of many body systems that minimize their energy are always interesting since they indicate which structures the systems will take at their ground states, reached as their temperature drops to 0 K. To simplify considerations, the interparticle interactions are often considered to be hard and thus the structure of the densest packing of hard particles becomes an essential issue in the theory of many real systems. When a system of many interacting particles is replaced by a single knotted filament, a similar question may still be asked: what is the conformation of its ground state? Here, the essential role is played by the filament self-interactions which determine its elastic properties. In the limit case, the self-interactions may be considered to be hard, leading to the notion of *perfect rope*, the details of which appear in the following section. Tying a knot with perfect rope, one may ask the essential question: what is the conformation at which the knot becomes tightest and its length reaches the global minimum? This question has also been considered using different models, e.g., for knots on the cubic lattice [1] and for nonoverlapping spheres [2]. Using the model of perfect rope, the only knot for which the length-minimizing (ideal as it is sometimes called) conformation is known is the trivial knot, i.e., the unknot. Its ropelength L, i.e., the ratio of the length of the rope to its radius, equals 2π. Ideal structures of a class of simple links, where each component is planar, were shown in [3]. Furthermore, a balance criterion [4] has made it possible to determine critical configurations for a simple clasp and for the Borromean rings [5,6]. One cannot prove that these configurations are ideal and the results rely on the assumption that the components are all planar and lie in perpendicular planes. Still, many researchers assume that these are ideal configurations. The exact structures of the ideal conformations of all other knots and links, and thus their minimal ropelengths, are not known. But here, as in the case of packing hard spheres, experiments, in particular numerical, provide essential insights. It is the aim of the present paper to describe and analyze the results of a series of numerical experiments performed with the use of the SONO algorithm [7], aimed at determining the minimum length of perfect rope which is sufficient to tie the simplest of the nontrivial knots: the trefoil knot.

In performing the experiments, we were aiming at two goals: (a) finding provable upper bounds for the ropelength of the trefoil knot and (b) finding, via an extrapolation procedure, an estimate of the lowest ropelength. The values of the upper bounds are of essential interest to the researchers working on the rigorous theory of ideal knots [8–12], while the value of the estimated least length is of interest to those studying the physical properties of knots. For example, to answer the basic question of how the tension within a knotted, thermally fluctuating filament depends on its length, we need to know the lowest possible value of the length. It may be also of use in the discussion of the length of knots found in the physical systems of a completely different nature [13].

II. THE PERFECT ROPE AND ITS CORRUGATED DISCRETE MODEL

To make the problem of tightening knots unambiguous we must specify a model of the rope on which the knots are tied. The simplest of such models is the *perfect rope*: perfectly flexible and at the same time perfectly hard. By perfectly flexible, we mean that it can be bent with zero force, thus, no elastic energy is stored in its bends. By perfectly hard, we mean that it cannot be squeezed, i.e., its perpendicular section always remains perfectly circular. We also assume that the surface of the rope is perfectly slippery. As a result, all changes to the conformation of the knot tied on the perfect rope need no force to be made and thus no potential energy is stored in the knot; it is also so in the case of the system of hard particles, e.g., spheres. One may ask about the relationship between the conformation of the knot found in the numerical experiments performed on a model rope and the conformations of the knot found in real, laboratory experiments. To answer this question, we again refer to the analogy with the problem of packing hard spheres. All real atoms are not hard spheres, but some of them, e.g., the atoms of noble gases, pack during crystallization into the fcc structure. This

*Electronic address: pieransk@man.poznan.pl
URL: http://fizyka.phys.put.poznan.pl/~pieransk/Personal.html
†Electronic address: rawdon@mathcs.duq.edu
URL: http://www.mathcs.duq.edu/~rawdon

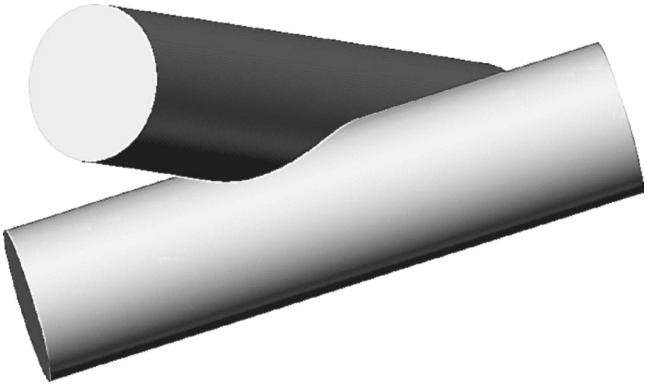

FIG. 1. When two pieces of the rope pass too close to each other, they overlap.

is so because in the packing process the spherical (the strongly repulsive) part of its mutual interaction plays the most essential role, and this part of the interaction can be replaced by the hard spherical repulsion in model systems. Real ropes are not perfect ropes but results we obtain in studying knots tied on the latter provide us with essential insights concerning knots tied on the former.

Let us describe in more detail the basic physical and geometrical properties of the perfect rope. We assume that its axis has no cusps; thus its tangent **t** is always well defined and continuous. This guarantees that its perpendicular sections are also well defined. We require that they always have the shape of disks of radius R where the centers of these disks are located on the rope axis K. Furthermore, the section disks are not allowed to overlap. This guarantees that the surface of the rope remains self-avoiding. Let us discuss the last condition in more detail.

The fact that two arclength-distant pieces of the perfect rope cannot be brought together to a distance smaller than $2R$ is obvious. Analyzing the situation in formal terms, we arrive at the conclusion that the doubly critical self-distance (i.e., the minimum distance between pairs of distinct points whose connecting chord is perpendicular to the tangents at both of the points) of the knot cannot be smaller than $2R$ [8]. When

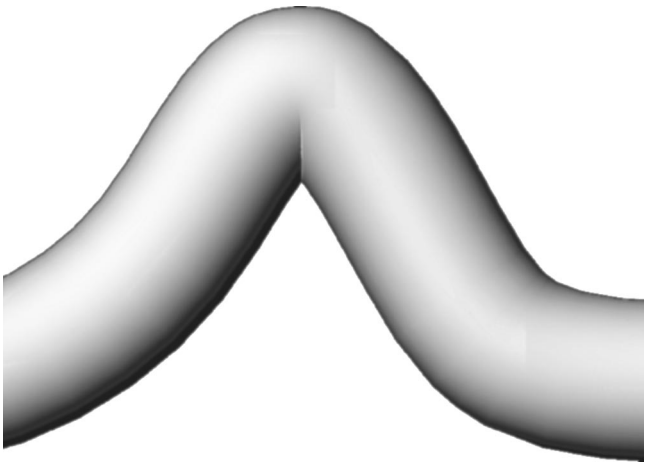

FIG. 2. When a bend in the rope is too sharp, its surface develops defects.

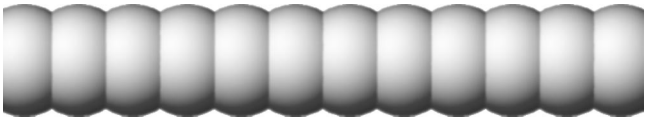

FIG. 3. Corrugated model of the perfect rope.

two portions of the thickened knot get too close, we have the situation shown in Fig. 1.

What is perhaps less obvious is what effect the self-avoiding condition places on the curving of its bends. The sharpness of a bend is described by the curvature κ of the rope axis. We assume that it cannot be higher than $1/R$. In other words, the radius of curvature can never be smaller than R. When the curvature is higher than $1/R$, we get the situation shown in Fig. 2.

To perform numerical experiments with knots tied on the perfect rope, we must first construct its discrete representation. We imagine that a continuous knot K is tied with perfect rope. It is represented in our simulations by a sequence of n points located on the rope axis. The points are indicated by vectors $\mathbf{v}_i$, $i=1,2,\ldots,n$. The points can be seen as vertices of a knotted polygon K_p. Because the knots that we are considering are closed, we implicitly take the subscript i modulo n. To simplify both the numerical calculations and their interpretation, we assume that consecutive vertices are equidistant with the common length of the edges denoted dl. Thus, K_p is an equilateral polygonal representation of K. Its edges will be treated as vectors

$$\boldsymbol{e}_i = \boldsymbol{v}_{i+1} - \boldsymbol{v}_i. \tag{1}$$

Let us emphasize that although all numerical simulations we perform deal with polygonal knots, their results can, as we shall demonstrate, be interpreted in terms of smooth knots. To simulate the hard shell of the perfect rope, we assume that each of the vertices of K_p is surrounded by a sphere of radius R. The union of all the spheres can be seen as a particular model of the perfect rope. Its surface is corrugated, with the corrugation vanishing with increasing numbers of vertices (i.e., as dl tends to zero). See Fig. 3. Figure 4 shows the tightest trefoil knot with $n=60$ vertices tied on the corrugated rope. One can see that in the middle region of the knot, the rope makes a short but distinct wiggle. In this region the

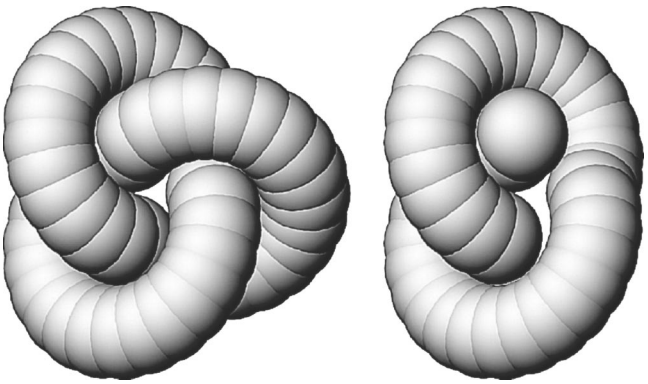

FIG. 4. The tightest trefoil knot tied on the corrugated rope consisting of $n=60$ cells.

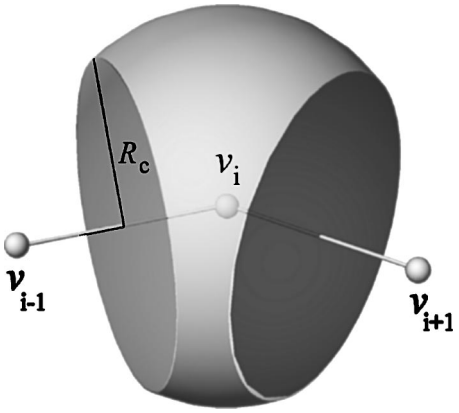

FIG. 5. Single cell of the corrugated rope.

curvature reaches its maximum; thus it must be carefully controlled for reasons described below. The corrugated rope is built from cells each of which can be seen as a piece of ball of radius R. See Fig. 5. Its flat side faces have the shape of disks of radius

$$R_c = \sqrt{R^2 - dl^2/4}. \tag{2}$$

As the rope is bent, the shapes of the cells change, becoming wedgelike. We assume that the bending is limited by the condition that the side disk faces of the cells are hard and thus they cannot overlap. Figure 6 shows the shape of the rope cell in the maximally bent situation. Simple trigonometric calculations show that the maximum bending angle is

$$\Theta_{\max} = 2 \arcsin\left(\frac{dl}{2R}\right). \tag{3}$$

Having defined the accessible shapes of the cells, we are able to define their mutual interaction simply as a hard one. As a result of this hard interaction, the corrugated rope always remains self-avoiding.

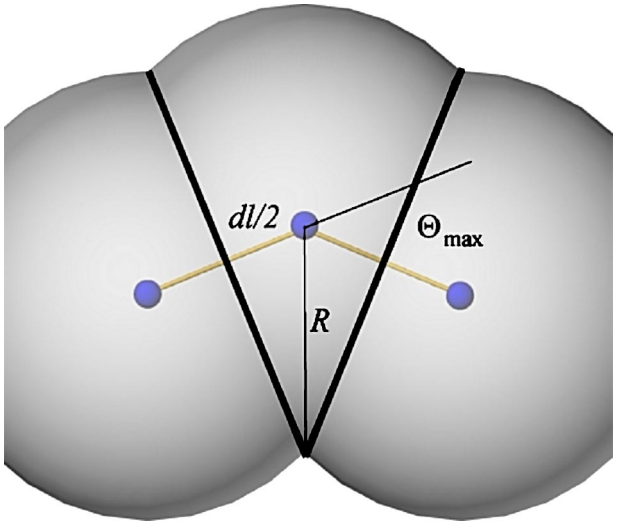

FIG. 6. The shape of the corrugated rope cell in the situation of maximal bending.

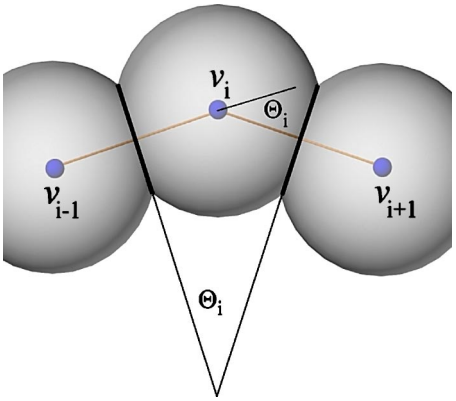

FIG. 7. Bending angle at the ith vertex.

III. NUMERICAL TIGHTENING: ALGORITHMS AND PROCEDURES

The numerical simulation of knots tightened on the corrugated rope must take care of two essential problems: (a) all cells of the rope should remain well defined, and (b) the cells should not overlap. To keep (a) satisfied, all bending angles

$$\Theta_i = \arcsin\frac{|\boldsymbol{e}_{i-1} \times \boldsymbol{e}_i|}{|\boldsymbol{e}_{i-1}||\boldsymbol{e}_i|} \tag{4}$$

must be determined and those of them which are larger than $\Theta_{\max}$ must be reduced. This is achieved by the application of the control curvature (CC) procedure which shifts the vertex $\boldsymbol{v}_i$ to a new position

$$\boldsymbol{v}_i' = \boldsymbol{v}_i + k_{CC}\frac{\boldsymbol{w}_i - \boldsymbol{v}_i}{|\boldsymbol{w}_i - \boldsymbol{v}_i|} \tag{5}$$

located closer to the middle point

$$\boldsymbol{w}_i = \frac{\boldsymbol{v}_{i-1} + \boldsymbol{v}_{i+1}}{2}, \tag{6}$$

located between vertices $\boldsymbol{v}_{i-1}$ and $\boldsymbol{v}_{i+1}$. The small factor k_{CC} is experimentally chosen. Usually it equals 0.001. See Fig. 7.

Such a reduction of the bending angle also reduces the lengths of edges $\boldsymbol{e}_{i-1}$ and $\boldsymbol{e}_i$. This and other disturbances to the lengths of edges is removed by the equalize edges (EE) procedure, which checks the distances between consecutive vertices and corrects them. One of a few correction algorithms we use has the following form:

$$\boldsymbol{v}_i' = \boldsymbol{v}_i - k_{EE}\frac{|\boldsymbol{e}_i| - dl}{|\boldsymbol{e}_i|}\boldsymbol{e}_i, \tag{7a}$$

$$\boldsymbol{v}_{i+1}' = \boldsymbol{v}_{i+1} + k_{EE}\frac{|\boldsymbol{e}_i| - dl}{|\boldsymbol{e}_i|}\boldsymbol{e}_i, \tag{7b}$$

where the k_{EE} factor controlling the efficiency of the EE procedure is experimentally chosen. Usually it equals 0.5.

Keeping (b) satisfied needs more attention. The problem we face here is that vertices whose index distance

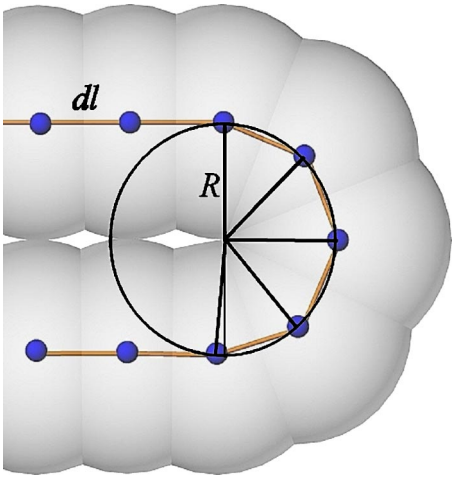

FIG. 8. The tightest turn of the corrugated rope.

$$D_I(\boldsymbol{v}_i,\boldsymbol{v}_j) = \begin{cases} |i-j| & \text{when } |i-j| \leqslant n/2, \\ n-|i-j| & \text{otherwise} \end{cases} \tag{8}$$

is smaller than $\pi R/dl$ should be allowed to stay closer than $2R$ (see [14] for a more detailed discussion, in particular with respect to the fact that the resulting knots are not exactly equilateral) since this is what happens when the rope enters the tightest turn. See Fig. 8. The distances between all pairs of vertices whose index distance exceeds this number should be larger than $2R$. If they are not, the vertices, say $\boldsymbol{v}_i$ and $\boldsymbol{v}_j$, are shifted away by the remove overlaps (RO) procedure according to the formulas

$$\boldsymbol{v}_i' = \boldsymbol{v}_i - k_{RO}\frac{2R-|\boldsymbol{v}_j-\boldsymbol{v}_i|+\epsilon}{|\boldsymbol{v}_j-\boldsymbol{v}_i|}(\boldsymbol{v}_j-\boldsymbol{v}_i), \tag{9a}$$

$$\boldsymbol{v}_j' = \boldsymbol{v}_i + k_{RO}\frac{2R-|\boldsymbol{v}_j-\boldsymbol{v}_i|+\epsilon}{|\boldsymbol{v}_j-\boldsymbol{v}_i|}(\boldsymbol{v}_j-\boldsymbol{v}_i), \tag{9b}$$

where the k_{RO} factor controlling the efficiency of the RO procedure is experimentally chosen. Usually it equals 0.5. The value of ϵ determines the excess distance by which the vertices are shifted apart. Its value, initially 10^{-3}, is reduced at the end of the tightening process to 10^{-8}. The actions of the CC, RO, and EE procedures are not consistent. Removing overlaps and controlling curvature disturbs the length of the edges, and vice versa, but in practice, at properly chosen values of the k_{CC}, k_{RO}, and k_{EE} factors, the multiple application of all the procedures leads to the common goal: an equilateral, overlap-free knot tied on the corrugated rope. The polygonal knot K_p can be seen as its skeleton.

The simulation of the tightening process runs as follows. When, as a result of the multiple application of the RO and EE procedures, the overlaps and the dispersion of the edge lengths are brought below an acceptable level, the vertices are moved by a small amount toward the centers of their osculating circles (Fig. 9). Let us explain what we mean here by the osculating circle. Consecutive edges $\boldsymbol{e}_{i-1},\boldsymbol{e}_i$ meet at the vertex $\boldsymbol{v}_i$. Being mostly noncollinear, they define a plane within which the (osculating) circle tangent to edges $\boldsymbol{e}_{i-1},\boldsymbol{e}_i$ at their midpoints is located. (The osculating circle will be used in the construction of the inscribed knot in the next section.) Let us denote the position of the center of the osculating circle by $\boldsymbol{O}_i$ and its radius by ρ_i. Thus, its curvature equals $\kappa_i=1/\rho_i$. Each vertex $\boldsymbol{v}_i$ is moved toward the center $\boldsymbol{O}_i$ of its osculating circle according to the formula

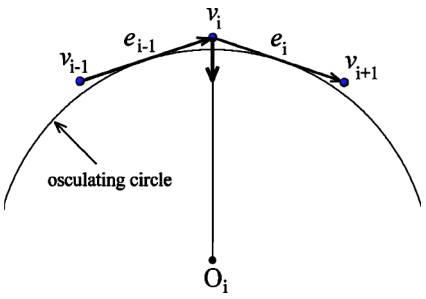

FIG. 9. During the tightening move of Eq. (10), each vertex is moved by a small amount toward the center of its osculating circle.

$$\boldsymbol{v}_i' = \boldsymbol{v}_i + c_{TM}\kappa_i\frac{\boldsymbol{O}_i-\boldsymbol{v}_i}{|\boldsymbol{O}_i-\boldsymbol{v}_i|}, \tag{10}$$

where c_{TM} is a small, experimentally adjusted parameter. Such a choice of the tightening algorithm is natural since it imitates what one would observe in reality if a knot submerged in a highly viscous medium were shrinking. Notice that this procedure of the SONO (shrink-on-no-overlaps) algorithm is different from the original one. It was first introduced in [15].

IV. INTERPRETATION OF RESULTS: FROM POLYGONAL TO SMOOTH KNOTS

The knot tightening simulation procedure delivers vertices of the polygonal knot K_p that can be seen as a skeleton of a tight knot tied on the corrugated rope. The problem we face is interpreting the result in terms of a knot tied on the C^1 smooth perfect rope. There is a simple way to do so. As shown in [14], the polygonal knot K_p can be replaced by the smooth knot K_c built from arcs inscribed into corners of K_p. The arcs, which we denote C_i, are tangent to the consecutive edges of K_p and connect in a C^1 smooth manner at their midpoints. The arc C_i is the portion of the osculating circle at $\boldsymbol{v}_i$ lying in the triangle formed by $\mathbf{v}_i$ and the midpoints of the two incident edges. The arc has total curvature equal to the bending angle at $\boldsymbol{v}_i$, i.e., Θ_i. The union of all the arcs is the smooth inscribed knot

$$K_c = \bigcup_{i=1}^{n} C_i. \tag{11}$$

See Fig. 10.

The knot K_c can be treated as the axis of a knot tied on the perfect rope of radius R_c. The circular arcs connect the centers of the disk-shaped faces and are perpendicular to them. Each of the arcs can be seen as the axis of a piece of the perfect rope of radius R_c, which is the common radius of all faces. The union of the tubes of radius R_c about the arcs C_i is the knot tied on the perfect rope. The rope as a whole is hidden inside the corrugated rope (except the circles where

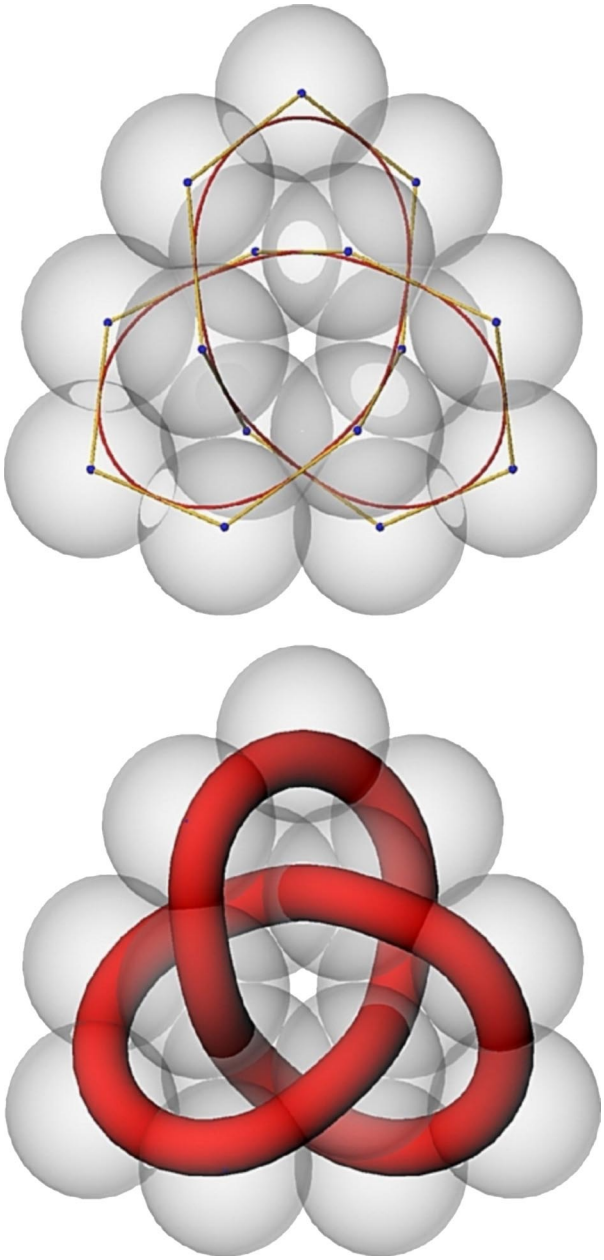

FIG. 10. Top: the polygonal K_p and inscribed K_c knots defined by the set of vertices delivered by the knot tightening algorithm. Bottom: the smooth inscribed knot K_c tied with the the perfect rope of radius R_c.

consecutive cells of the corrugated rope meet; here the corrugated rope and the perfect rope coincide). In view of the above, the knot K_c tied on the perfect rope is self-avoiding. See Fig. 10. For a formal proof see [14].

Let us describe some interesting properties of the inscribed knot K_c. Due to its construction, it is piecewise C^2 (and thus $C^{1,1}$) since its tangent vector $\mathbf{t}$ is everywhere well defined and continuous, and the curvature is defined at all but a finite number of points, namely, at the midpoints of the edges of K_p. Being built from circular arcs of various curvature radii ρ_i, it has piecewise-constant curvature. Since the arcs are planar curves, but the planes within which they are located are in general not coplanar, its torsion τ is a sum of

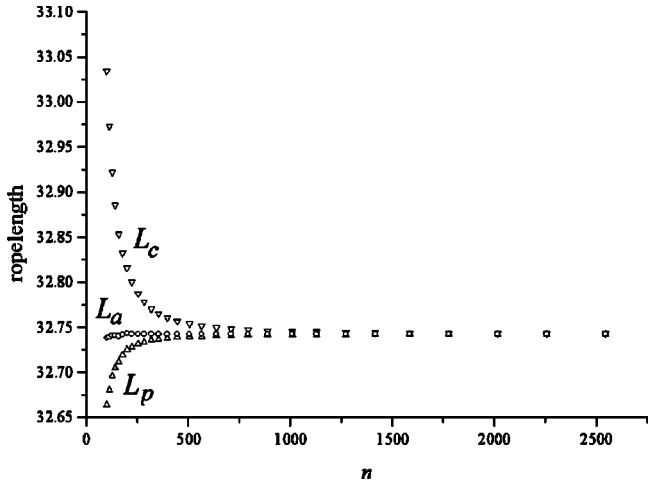

FIG. 11. The raw polygonal L_p, inscribed L_c, and weighted average L_a ropelengths of the tightest SONO trefoil knots tied on the corrugated rope versus the number of vertices.

Dirac δ functions localized at the points at which the consecutive arcs meet. Their weights are equal to the angles between consecutive osculating planes.

V. THE RAW POLYGONAL AND THE INSCRIBED ROPELENGTHS

The problem we face now is how to determine the $n \to \infty$ limiting length-to-radius ratio of the knot whose discrete representations, for a sequence of increasing n, are tightened by the simulation program. For each n, the program delivers vertices $\mathbf{v}_i$ of the polygonal knot K_p. Since the spheres used in the construction of the corrugated rope have radius R, we may assume that the radius of the rope equals R. To normalize the results, we assume for the remainder of this paper that $R=1$.

The normalized length, which we shall refer to as the *raw ropelength*, of the corrugated rope knot can be found simply by adding lengths of all edges of its polygonal skeleton K_p. Since K_p is (within the accepted error range) equilateral, its raw ropelength is

$$L_p = \sum_{i=1}^{n} |\mathbf{v}_{i+1} - \mathbf{v}_i| \approx ndl. \tag{12}$$

Another way of finding the ropelength is summing up the lengths $L(C_i)$ of all circular arcs forming the inscribed knot K_c and dividing the value by the radius R_c:

$$L_c = \frac{1}{\sqrt{1 - dl^2/4}} \sum_{i=1}^{n} L(C_i). \tag{13}$$

Since we know that the smooth ropelength of K_c does not exceed L_c, the *inscribed ropelength* L_c will overestimate the minimum ropelength L_∞. See Fig. 10.

To approximate the value of L_∞, we performed a series of knot tightening simulations on the trefoil knot with n ranging from 99 to 2544. Figure 11 presents the results of the ropelengths L_p and L_c found for these knots. Indeed, the raw

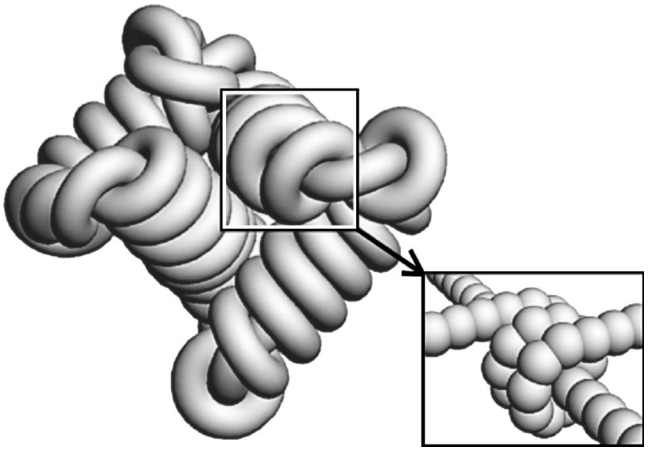

FIG. 12. A tight conformation of the (59,2) torus knot.

polygonal and the inscribed ropelengths are seen to converge with increasing n to a common value: the former from below, the latter from above. Having obtained these results, is it possible to determine the common limit value, i.e., SONO's best approximation for the ropelength of an ideal trefoil knot? To solve the problem, we first tried to see if a properly weighted average could deliver values whose dependence on n would be weaker than the dependencies of L_p and L_c. Simple experiments reveal that the weighted average

$$L_a = \frac{(4L_p + L_c)}{5} \tag{14}$$

provides values almost independent of n. The data shown in Fig. 11 illustrate this.

VI. MODEL ANALYSIS OF THE WEIGHTED AVERAGE ROPELENGTH

The minimal dependence of L_a on n suggests that it could result from some simple properties of L_p and L_c. Thus we performed an analytical analysis on a model situation. The trefoil knot belongs to the family of $(m,2)$ torus knots. Figure 12 shows a tight (59, 2) knot from this family. As seen in the figure, the most characteristic structure which appears in such knots in a tight conformation is a tight winding of a helical structure about an almost straight line. Thus, we decided to analyze this model situation.

When a corrugated rope winds tightly around a straight piece of the same corrugated rope, it travels through its valleys and hills. A similar situation happens when a corrugated torus is shifted along a corrugated tube. This latter system is simple enough to be analyzed rigorously. Thus, we determined how L_p and L_c of the torus behave in the model case.

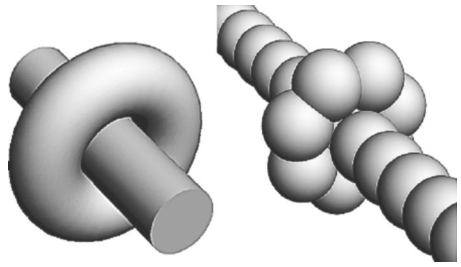

FIG. 13. The tightest torus wound around a straight rope; the smooth and corrugated cases.

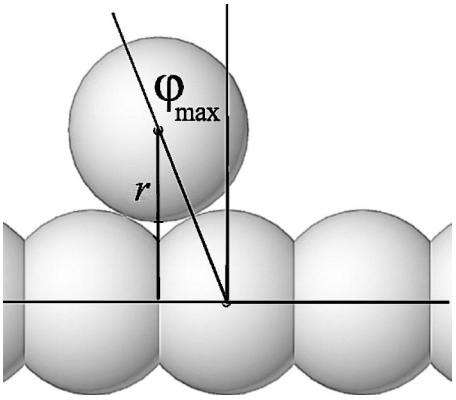

FIG. 14. Position of one of the spheres, of which the corrugated torus is constructed, is controlled by the angle φ. In the picture, the angle has its maximum value $\varphi_{\max}$.

First notice that we know the exact value of L_∞ in this case. When both the torus and the rope on which it is tightly wound are smooth, the length of the torus is 4π, which is the desired L_∞ value in this situation. See Fig. 13. Recall that we are assuming $R=1$.

Now, let us consider the corrugated rope case. Here, a corrugated torus winds around the corrugated rope. Let us assume that the number of spherical cells of which the corrugated torus is built equals n. The skeleton of the corrugated torus is a regular n-gon. The length dl of its edges depends on the position of the straight corrugated rope at which it is wound: dl is smallest when the corrugated torus is located in the groove and highest when it is located on the hill. Its position can be described by the angle φ as shown in Fig. 14. The distance of the vertices of the corrugated torus from the axis of the corrugated straight rope is denoted by r. See Fig. 15. This distance depends on φ and is

$$r = 2\cos(\varphi). \tag{15}$$

The value of r reaches its minimum $r_{\min}$, when φ is at its maximum $\varphi_{\max}$:

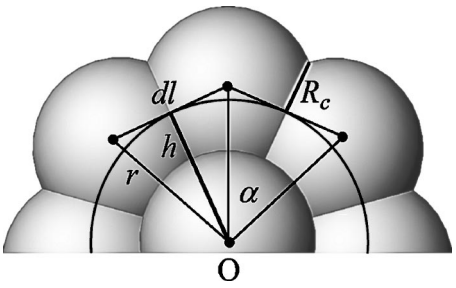

FIG. 15. Geometry of the n-gon skeleton of the corrugated torus.

$$r_{\min} = 2\cos(\varphi_{\max}). \tag{16}$$

Knowing r, we may find the length dl of the edges of the corrugated torus,

$$dl = 2r\sin\left(\frac{\pi}{n}\right) = 4\cos(\varphi)\sin\left(\frac{\pi}{n}\right). \tag{17}$$

Notice that in the model, we are considering the edge length of the corrugated straight rope around which the torus is tightly wound, which also equals dl. The value of dl reaches its minimum when the torus is in the groove, i.e., when φ is at its maximum:

$$dl_{\min} = 4\cos(\varphi_{\max})\sin\left(\frac{\pi}{n}\right). \tag{18}$$

The maximum value that the angle φ can reach is given by solution of the equation

$$\sin(\varphi_{\max}) = \frac{dl_{\min}}{4} \tag{19}$$

which in view of Eq. (18) takes the following form:

$$\sin(\varphi_{\max}) = \cos(\varphi_{\max})\sin\left(\frac{\pi}{n}\right). \tag{20}$$

Thus,

$$\varphi_{\max} = \arctan\left[\sin\left(\frac{\pi}{n}\right)\right]. \tag{21}$$

Knowing the limit value of φ, we may find the average value of r,

$$\overline{r} = \frac{\int_0^{\varphi_{\max}} r\, d\varphi}{\varphi_{\max}} = \frac{2\sin(\pi/n)}{\arctan[\sin(\pi/n)]\sqrt{1+\sin^2(\pi/n)}}. \tag{22}$$

The skeleton of the corrugated torus is an n-gon. At the average value of r, the length of its edges equals

$$\overline{dl} = 2\overline{r}\sin\left(\frac{\pi}{n}\right). \tag{23}$$

See Fig. 15. Thus, the raw polygonal length of the corrugated torus is given by

$$L_p(n) = n\,\overline{dl} = 4n\frac{\sin^2(\pi/n)}{\arctan^2[\sin(\pi/n)]\sqrt{1+\sin^2(\pi/n)}}. \tag{24}$$

Now, let us inscribe into the n-gon a smooth curve built from inscribed arcs in the same manner as we did in considering polygonal knots. Here, at the average value of r, the curve is simply a circle of radius

$$\overline{h} = \sqrt{\overline{r^2} - \frac{\overline{dl^2}}{4}} \tag{25}$$

of length

$$L_c'(n) = 2\pi\overline{h}. \tag{26}$$

The circle can be seen as the axis of a smooth rope of radius

$$R_c = \sqrt{1 - \frac{\overline{dl^2}}{4}}. \tag{27}$$

Eventually, the dependence of its ropelength on n is given by the expression

$$L_c(n) = \frac{L_c'}{R_c} = 4\pi\sqrt{\frac{\sin^2(\pi/n) - \sin^4(\pi/n)}{[1+\sin^2(\pi/n)]\arctan^2[\sin(\pi/n)] - 4\sin^4(\pi/n)}} \tag{28}$$

which looks rather complex, but when expanded into a series, in terms of $1/n$, reveals a rather simple dependence on n:

$$L_c(n) = 4\pi + \frac{16}{3}\pi^3\frac{1}{n^2} + O\left(\frac{1}{n^4}\right). \tag{29}$$

Similarly, the dependence $L_p(n)$ can be expanded into series in terms of $1/n$ giving

$$L_p(n) = 4\pi - \frac{4}{3}\pi^3\frac{1}{n^2} + O\left(\frac{1}{n^4}\right). \tag{30}$$

From the above formulas, one can immediately see that (1) as expected, both L_p and L_c tend with increasing n to the $L_\infty = 4\pi$ value; (2) at finite n, L_p underestimates the ropelength of the torus, while L_c overestimates it; and (3) the weighted average of the expansions $L_a = (4L_p + L_c)/5$ better approximates L_∞.

The last conclusion is essential, since it supports the experimental results that the weighted average of the numerically found ropelengths L_p and L_c displays a weak dependence on the number of vertices and thus allows one to provide good estimates of the L_∞ ropelength of the knots even at small n.

By analyzing more carefully the deviations of L_p and L_c from the proper L_∞ value, we may conclude that their magnitude depends both on n and on the value of L_∞; what matters here is the ratio L_∞/n. Thus, the most natural function describing the dependence of L_p and L_c on n should have the form

$$L_\infty\left[1 + b\left(\frac{L_\infty}{n}\right)^2\right]. \tag{31}$$

Taking into account that in our case $L_\infty = 4\pi$, we may transform the formulas (29) and (30) to the form

$$L_c = 4\pi\left[1 + \frac{1}{12}\left(\frac{4\pi}{n}\right)^2\right], \tag{32a}$$

$$L_p = 4\pi\left[1 - \frac{1}{48}\left(\frac{4\pi}{n}\right)^2\right]. \tag{32b}$$

Thus, in the case of L_c the b parameter equals $1/12$, while for L_p it is $-1/48$. Below we analyze the results of the numerical simulations carried out on the trefoil knot to see if we obtain similar results.

TABLE I. Numerically found ropelengths of the tightest SONO trefoil knot tied on the corrugated rope with various numbers of vertices.

n	L_p	L_c	$L_a=(4L_p+L_c)/5$
99	32.6647176	33.0345690	32.73868788
111	32.6812344	32.9733664	32.73966080
126	32.6962424	32.9221906	32.74143204
141	32.7053340	32.8859212	32.74145144
159	32.7124892	32.8533314	32.74065764
177	32.7194584	32.8330050	32.74216772
198	32.7256180	32.8164914	32.74379268
222	32.7285652	32.8006428	32.74298072
252	32.7319694	32.7878064	32.74313680
282	32.7341496	32.7786866	32.74305700
318	32.7359878	32.7710046	32.74299116
354	32.7372462	32.7654718	32.74289132
396	32.7384826	32.7610420	32.74299448
444	32.7393900	32.7573132	32.74297464
504	32.7401800	32.7540806	32.74296012
564	32.7407196	32.7518186	32.74293940
636	32.7412068	32.7499328	32.74295200
708	32.7415512	32.7485920	32.74295936
792	32.7418288	32.7474540	32.74295384
888	32.7420514	32.7465248	32.74294608
1008	32.7422584	32.7457310	32.74295292
1128	32.7424006	32.7451740	32.74295528
1272	32.7425154	32.7446960	32.74295152
1416	32.7425976	32.7443568	32.74294944
1584	32.7426692	32.7440750	32.74295036
1776	32.7427278	32.7438460	32.74295144
2016	32.7427756	32.7436436	32.74294920
2256	32.7428132	32.7435064	32.74295184
2544	32.7428414	32.7433864	32.74295040

VII. RESULTS

Following suggestions provided by the analysis presented above, we performed a series of SONO knot tightening simulations on the trefoil knot with the number of vertices ranging from $n=99$ up to $n=2544$. The results of the simulations, i.e., the values of L_p, L_c, and L_a, are presented in Table I and in Fig. 11. The data are presented in the table with an excessive accuracy just to show at which decimal digits the values, in particular L_a, are changing.

To find the L_∞ value, we have taken into consideration the last nine points, i.e., the data obtained for $n=1008$, 1128, 1272, 1416, 1584, 1776, 2016, 2256, and 2544. As suggested by results of the model analysis performed above, the L_p and L_c data were fitted with the function from (31). See Fig. 16.

The value of the L_∞ fitting parameter proved to be identical for both ropelengths. Its value equals $32.742\,950\pm0.000\,001$. Values of the b parameter were found to be $-0.019\,98$ and $0.080\,54$ for fits of the L_p and L_c data, respectively. Furthermore, the values are not far from the values predicted by the model analysis: $-1/48\approx-0.020\,83$ and $1/12\approx0.083\,33$. When a knot or link has much of its self-contact resulting from helical-like wrapping, such as the (59,2) torus knot in Fig. 12, we would expect the fitting parameters to be close to those predicted by the torus analysis. However, for most knots and links, this very well may not be the case. Further analysis is necessary to determine how well this technique will work for other knots and links.

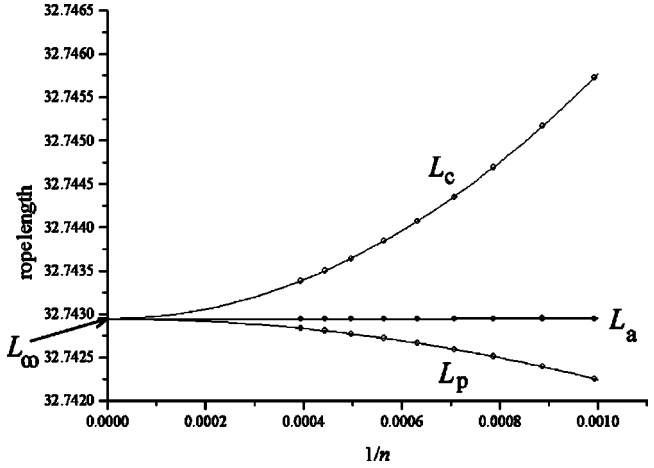

FIG. 16. Polygonal, inscribed, and weighted average ropelengths of the tightest trefoil knots tied on the corrugated rope versus the inverse of the number of vertices. Curves shown in the figure were obtained by fitting the data with the function given by (31).

VIII. DISCUSSION

Numerical simulations of the knot tightening process for a perfect rope provide us with ropelength data which can be used to determine an estimate of the ideal knot ropelength. The simulations of the knot tightening process that we presented above were based on a modified SONO algorithm. Analyzing the trefoil conformations it provided, we found that as the number of the vertices tends to infinity, the raw and inscribed ropelength fitting curves converge to $L_\infty=32.742\,950\pm0.000\,001$. A word of caution seems necessary. The L_∞ value was obtained by extrapolation of the ropelength data found for the increasing number of vertices. The data end at $n=2544$. One cannot exclude, although it seems highly unlikely, that for a higher value of n the conformation of the trefoil will undergo a qualitative change to a better, i.e., smaller ropelength, form. Thus, from the rigorous point of view, the 32.742 950 value is only an estimate of the ideal trefoil ropelength.

On the other hand, the L_c values presented in Table I can be interpreted differently. Each of them is a numerically found, provable upper bound of the trefoil ropelength up to computer round-off error. Thus, the smallest of these, $L_c=32.743\,386\,4$, found at $n=2544$ is the lowest known provable upper bound of the trefoil ropelength. This is an improvement on the upper bounds 32.77 [9], 32.744 46 [11,12], and 32.743 91 [14]. The value is smaller than the value ob-

tained previously with the original SONO algorithm [14]. One cannot exclude that different tightening algorithms will be able to find still better, i.e., smaller, values of the essential geometrical parameter of knots, but so far the value we have found is smallest. Our bound can also be compared to the rigorous lower bound 31.32 found recently by Denne, Diao, and Sullivan [10]. Having both bounds, we know that the ropelength of the ideal trefoil is located somewhere between these values, although the actual value is most likely closer to the numerical upper bound.

Numerical simulations performed with the use of the SONO algorithm provide us with coordinates of vertices of equilateral polygonal knots. As we have shown, the vertices can be used to construct smooth, piecewise constant curvature knots. Such knots have a direct physical sense since, in principle, they can be assembled with pieces of a tube. For instance, looking at Table I one can see that to construct a 99-piece knot, one should take 33.034 569 inches of 1-in. radius tubing, cut it into pieces of appropriate length, bend the pieces into appropriate constant curvature elements, and carefully connect them to match the angle between their osculating planes; these connection points are where the torsion of the knot is accumulated. It seems obvious that allowing the pieces of the tube to have a variable curvature and nonzero torsion will allow one to reduce their length further. Finding the exact shapes of the pieces with which an ideal trefoil can be constructed needs rigorous analysis and thus remains still a distant goal.

ACKNOWLEDGMENTS

P.P. thanks Maciej Oszwaldowski for indicating the possibility of the analytical treatment of the corrugated torus model. The authors thank John Sullivan for many helpful comments. J.B., P.P., and S.P. acknowledge financial support by Grant No. PB-62-204/04-BW, and E.J.R. by NSF Grant No. 0311010.

[1] Y. Diao, J. Knot Theory Ramif. **2**, 413 (1993).
[2] R. Kusner and W. Kusner (unpublished).
[3] J. Cantarella, R. B. Kusner, and J. M. Sullivan, Invent. Math. **150**, 257 (2002).
[4] J. Cantarella, J. Fu, R. Kusner, J. Sullivan, and N. Wrinkle (unpublished).
[5] J. Cantarella, J. Fu, R. Kusner, J. Sullivan, and N. Wrinkle, e-print math.DG/0402212.
[6] E. Starostin, Forma **18**, 263 (2003).
[7] P. Pierański, Pro Dialog **5**, 111 (1997) (in Polish).
[8] R. A. Litherland, J. Simon, O. Durumeric, and E. Rawdon, Topol. Appl. **91**, 233 (1999).
[9] E. J. Rawdon, Exp. Math. **12**, 287 (2003).
[10] E. Denne, Y. Diao, and J. M. Sullivan, e-print math.DG/0408026.
[11] J. Smutny, Ph.D. thesis, École Polytechnique Fédérale de Lausanne, 2004.
[12] M. Carlen, B. Laurie, J. H. Maddocks, and J. Smutny (unpublished).
[13] A. Malevanets and R. Kapral, Phys. Rev. Lett. **77**, 767 (1996).
[14] J. Baranska, P. Pieranski, and E. J. Rawdon, e-print physics/0409108.
[15] S. Przybyl, Ph.D. thesis, Poznan University of Technology, 2001 (in Polish).